

# UCSF

## UC San Francisco Previously Published Works

### Title

Investigating the clinico-anatomical dissociation in the behavioral variant of Alzheimer disease

### Permalink

<https://escholarship.org/uc/item/1dd0r82d>

### Journal

Alzheimer's Research & Therapy, 12(1)

### ISSN

1758-9193

### Authors

Singleton, Ellen H

Pijnenburg, Yolande AL

Sudre, Carole H

et al.

### Publication Date

2020-12-01

### DOI

10.1186/s13195-020-00717-z

### Copyright Information

This work is made available under the terms of a Creative Commons Attribution License, available at <https://creativecommons.org/licenses/by/4.0/>


Peer reviewed

RESEARCH

Open Access



# Investigating the clinico-anatomical dissociation in the behavioral variant of Alzheimer disease

Ellen H. Singleton<sup>1\*</sup> , Yolande A. L. Pijnenburg<sup>1</sup>, Carole H. Sudre<sup>2</sup>, Colin Groot<sup>1</sup>, Elena Kochova<sup>1</sup>, Frederik Barkhof<sup>3,4</sup>, Renaud La Joie<sup>5</sup>, Howard J. Rosen<sup>5</sup>, William W. Seeley<sup>5</sup>, Bruce Miller<sup>5</sup>, M. Jorge Cardoso<sup>2,6</sup>, Janne Papma<sup>7,8</sup>, Philip Scheltens<sup>1</sup>, Gil D. Rabinovici<sup>5,9,10,11</sup> and Rik Ossenkoppele<sup>1,12</sup>

## Abstract

**Background:** We previously found temporoparietal-predominant atrophy patterns in the behavioral variant of Alzheimer's disease (bvAD), with relative sparing of frontal regions. Here, we aimed to understand the clinico-anatomical dissociation in bvAD based on alternative neuroimaging markers.

**Methods:** We retrospectively included 150 participants, including 29 bvAD, 28 "typical" amnesic-predominant AD (tAD), 28 behavioral variant of frontotemporal dementia (bvFTD), and 65 cognitively normal participants. Patients with bvAD were compared with other diagnostic groups on glucose metabolism and metabolic connectivity measured by [<sup>18</sup>F]FDG-PET, and on subcortical gray matter and white matter hyperintensity (WMH) volumes measured by MRI. A receiver-operating-characteristic-analysis was performed to determine the neuroimaging measures with highest diagnostic accuracy.

**Results:** bvAD and tAD showed predominant temporoparietal hypometabolism compared to controls, and did not differ in direct contrasts. However, overlaying statistical maps from contrasts between patients and controls revealed broader fronto-insular hypometabolism in bvAD than tAD, partially overlapping with bvFTD. bvAD showed greater anterior default mode network (DMN) involvement than tAD, mimicking bvFTD, and reduced connectivity of the posterior cingulate cortex with prefrontal regions. Analyses of WMH and subcortical volume showed closer resemblance of bvAD to tAD than to bvFTD, and larger amygdalar volumes in bvAD than tAD respectively. The top-3 discriminators for bvAD vs. bvFTD were FDG posterior-DMN-ratios (bvAD < bvFTD), MRI posterior-DMN-ratios (bvAD < bvFTD), MRI salience-network-ratios (bvAD > bvFTD, area under the curve [AUC] range 0.85–0.91, all  $p < 0.001$ ). The top-3 for bvAD vs. tAD were amygdalar volume (bvAD > tAD), MRI anterior-DMN-ratios (bvAD < tAD), FDG anterior-DMN-ratios (bvAD < tAD, AUC range 0.71–0.84, all  $p < 0.05$ ).

**Conclusions:** Subtle fronto-insular hypometabolism and anterior DMN involvement may underlie the prominent behavioral phenotype in bvAD.

**Keywords:** Alzheimer's disease, Behavior, Frontotemporal dementia, MRI, PET

\* Correspondence: [e.singleton@amsterdamumc.nl](mailto:e.singleton@amsterdamumc.nl)

<sup>1</sup>Alzheimer Center Amsterdam, Department of Neurology, Amsterdam Neuroscience, Vrije Universiteit Amsterdam, Amsterdam UMC, Amsterdam, the Netherlands

Full list of author information is available at the end of the article



© The Author(s). 2020 **Open Access** This article is licensed under a Creative Commons Attribution 4.0 International License, which permits use, sharing, adaptation, distribution and reproduction in any medium or format, as long as you give appropriate credit to the original author(s) and the source, provide a link to the Creative Commons licence, and indicate if changes were made. The images or other third party material in this article are included in the article's Creative Commons licence, unless indicated otherwise in a credit line to the material. If material is not included in the article's Creative Commons licence and your intended use is not permitted by statutory regulation or exceeds the permitted use, you will need to obtain permission directly from the copyright holder. To view a copy of this licence, visit <http://creativecommons.org/licenses/by/4.0/>. The Creative Commons Public Domain Dedication waiver (<http://creativecommons.org/publicdomain/zero/1.0/>) applies to the data made available in this article, unless otherwise stated in a credit line to the data.

## Background

Individuals with the behavioral variant of Alzheimer's disease (bvAD) present with early and prominent behavioral and personality changes, with AD as the primary etiology [1]. Case reports and small sample studies have suggested prominent frontal atrophy and pathology in bvAD patients [2–5]. The largest neuroimaging study to date in clinically defined bvAD patients revealed a prominent temporoparietal atrophy pattern with a relative lack of frontal atrophy [1], questioning the neurobiological basis of the prominent behavioral deficits. The behavioral phenotype in these individuals might be explained better by complementary neuroimaging techniques. For example, functional measures such as glucose hypometabolic patterns or alterations in metabolic connectivity may be more sensitive than structural MRI [6] and allow the assessment of large-scale networks rather than sole investigation of localized associations [7]. Furthermore, structural measures such as subcortical atrophy or white matter damage affecting frontosubcortical tracts have consistently been associated with neuropsychiatric symptoms [8, 9]. Exploring these neuroimaging features will enhance our neurobiological understanding of the prominently behavioral phenotype in bvAD. In addition, it may aid the often challenging differential diagnosis of bvAD versus “typical” AD or the behavioral variant of frontotemporal dementia (bvFTD) [5, 10], and potentially lead to more accurate diagnoses and patient management. We had two objectives: (i) to increase our understanding of the relative lack of frontal atrophy in patients with the behavioral variant of AD through the assessment of multiple neuroimaging markers and (ii) to identify the diagnostic accuracy of several neuroimaging measures in the differential diagnosis of bvAD vs. typical AD and bvFTD.

## Methods

### Participants

From our initial bvAD paper [1], we included 33 bvAD patients from the University of California San Francisco (UCSF) Aging and Dementia Research Center (ADRC; San Francisco, USA). From this selection, we included all patients that had FDG, FLAIR-MR, or T1-MR images available ( $n = 32$ ). There were 29 bvAD patients with research quality MR data, 19 with FDG-PET, and 15 with FLAIR-MRI (see Supplement 1 for overviews of data availability and Supplement 2 for characteristics of the T1-MRI, FDG-PET, and FLAIR-MRI subsets respectively). In the absence of consensus clinical criteria for the behavioral variant of AD, patients with bvAD were defined retrospectively by a group of behavioral neurologists (G.D.R., Y.A.L.P., P.S.) and neuropsychologists (R.O., J.H.K.) as patients with a diagnosis of bvFTD or “frontal variant AD” or a differential diagnosis of bvFTD vs. AD who had biomarker evidence for and/or autopsy confirmation of AD pathology [1]. Patients

with bvAD were matched with 28 tAD patients and 28 bvFTD patients, also described in the original study [1]. tAD patients fulfilled criteria for probable AD with at least an intermediate-likelihood of AD pathophysiology according to the National Institute on Ageing-Alzheimer's Association criteria [11] or mild cognitive impairment due to AD [12] based on positive amyloid biomarkers and/or autopsy. bvFTD patients met the clinical criteria proposed by Neary and colleagues [13] or Rascovsky and colleagues [14] and had negative amyloid biomarkers and/or autopsy confirmation. Patients with significant cerebrovascular disease were excluded from the UCSF-ADRC. Finally, we selected two cognitively normal control groups. The first group underwent MRI on the same scanners as the patients at UCSF, but had no FDG-PET data available (CN<sub>1</sub>,  $n = 34$ ). The second group underwent FDG-PET on the same scanners as the patients at the University of California Berkeley (CN<sub>2</sub>,  $n = 31$ ), but had MRI on a different scanner than the patients. Both CN groups had cognitive test scores within the normal range and absence of neurological or psychiatric illness [15].

### Neuroimaging markers in bvAD

#### Glucose hypometabolism

FDG-PET images were obtained at Lawrence Berkeley National Laboratory (LBNL) using a Siemens ECAT-EXACT-HR-PET ( $n_{\text{bvAD}} = 15$ ) or Biograph PET/CT ( $n_{\text{bvAD}} = 4$ ) scanner. Acquisition parameters have been specified elsewhere [16]. Starting 30 min post-injection of 5–10 mCi of [<sup>18</sup>F] Fluorodeoxyglucose (FDG), 6 × 5 minutes frames of emission data were collected. All PET data were reconstructed using an ordered subset expectation maximization algorithm with weighted attenuation. Images were smoothed with a 4 × 4 × 4-mm Gaussian kernel with scatter correction. FDG-PET frames of 30–60 min post-injection aligned to the first frame and averaged. Next, each frame was realigned to the resultant mean image. These native space images were summed, and standardized uptake value ratios (SUV<sub>r</sub>) were calculated by normalizing the summed FDG images to the mean activity in the pons, as glucose metabolism in this region has been shown to be preserved in AD [17]. A mutual information affine registration was used to coregister these normalized FDG-PET images to the corresponding MRI in native space. For the cognitively normal group with FDG-PET scans available (CN<sub>1</sub>), MRI scans were obtained on a 1.5T Magnetom Avanto System scanner (Siemens Inc., Iselin, NJ) at the University of Berkeley, with a 12-channel head coil run in triple mode. These images were used for PET processing only. Subsequently, the MRIs were registered to Montreal Neurological Institute (MNI) space and the FDG-PET images were then also transformed to MNI space using the individual deformation fields obtained from the

coregistered MRI normalization. The normalized FDG-PET images were then smoothed using a 12-mm Gaussian kernel [18]. All images were visually inspected and deemed suitable for further analyses. Then, voxel-wise comparisons of FDG-SUVr images were performed in SPM12 (Wellcome Trust Center for Neuroimaging, University College London, [www.fil.ion.ucl.ac.uk/spm](http://www.fil.ion.ucl.ac.uk/spm)), using an analysis of covariance model that included age and sex as covariates. Pairwise contrasts were performed among the four groups (i.e., bvAD, tAD, bvFTD, and CN<sub>1</sub>), which yields *T*-maps signifying the difference in SUVr for each voxel. For comparisons between patients and controls, we thresholded *T*-maps at  $p < 0.05$ , family-wise error (FWE) corrected, and an extent threshold of  $k = 50$  voxels. For contrasts between patient groups, we applied an uncorrected threshold of  $p < 0.001$  and extent threshold of  $k = 50$  voxels due to smaller expected differences between groups. This yields binary maps of significant voxels for each comparison and we overlaid these maps for patients vs. control contrasts on an MNI brain template to visualize regional differences and overlap between groups. To allow a head-to-head comparison between FDG-PET hypometabolic patterns and MRI atrophy patterns, we performed voxel-based morphometry on the individuals that had both FDG-PET and MRI available. Patients vs patients contrasts were assessed at  $p_{\text{uncorrected}} < 0.001$ ,  $k = 50$  extent threshold, and patients vs controls contrasts were examined at  $p_{\text{FWE}} < 0.05$ ,  $k = 50$  extent threshold, correcting for age, sex, total intracranial volume, and scanner field strength. See the “Subcortical atrophy” section for a description of MRI methods.

#### Metabolic connectivity—goodness-of-fit analysis

Resting-state metabolic connectivity was examined in all groups using a voxel-wise interregional correlation analysis (IRCA) of FDG-PET data [19]. This method involved several steps [20]: (i) selection of relevant networks, (ii) definition of seed regions-of-interest (ROI) within key regions in these functional networks as described in previous literature, (iii) generation of covariance maps by correlating the mean FDG-SUVr in the seed ROI with the mean FDG-SUVr in all voxels across the brain, and (iv) comparing these covariance maps to functional network templates and calculating goodness-of-fit (GOF) scores for each network. For step (i), we selected networks from the literature that are thought to play a pivotal role in bvFTD and tAD [21], including the default mode network (DMN) [22], salience network (SN) [23], and executive control network (ECN) [24]. To study the specific contribution of posterior vs. anterior DMN, the DMN was fractioned into anterior and posterior subsystems in accordance with previous studies [25–27]. For step (ii), the left posterior cingulate cortex (PCC, MNI coordinates:  $x = -8$ ,  $y = -56$ ,  $z = 26$  [25]) was

selected as the seed region for the posterior DMN, the left anterior medial prefrontal cortex (amPFC,  $x = 6$ ,  $y = 52$ ,  $z = -2$  [25]) for the anterior DMN, the right frontoinsula (riFI,  $x = 36$ ,  $y = 18$ ,  $z = 4$  [28]) for the SN, and the right dorsolateral prefrontal cortex (riDLPFC,  $x = 44$ ,  $y = 36$ ,  $z = 20$  [24]) for the ECN. Spheres of 4 mm were drawn around the abovementioned coordinates and, for each subject, mean FDG SUVr values were extracted from each of these spheres using Marsbar while using a gray matter mask to exclude PET counts from white matter and cerebrospinal fluid. For step (iii), multiple linear regressions were performed in SPM12 to assess correlations between FDG uptake in each seed ROI and FDG uptake across the brain, resulting in interregional covariance maps. As the PET covariance analyses explored correlations between the seed region and each voxel *across subjects*, one interregional correlation map was obtained per group. The interpretation of these maps is based on the notion that regions covarying in levels of metabolism are associated to each other. Separate models were used for each group, resulting in four interregional covariance maps per group. These analyses were adjusted for age and sex. For step (iv), the goodness-of-fit of the interregional covariance maps with standard functional network templates, published by the Stanford Functional Imaging in Neuropsychiatric Disorders Lab [29], was assessed. As previously described [29], these standard functional network templates were created by applying FSL's MELODIC independent component analysis software to resting state fMRI data of 15 healthy control subjects. The network templates were downloaded as binary ROIs from [http://findlab.stanford.edu/functional\\_ROIs.html](http://findlab.stanford.edu/functional_ROIs.html). Goodness-of-fit was assessed by calculating the difference between the mean *T*-score of all voxels of the interregional covariance map (transformed SPM *T*-maps) inside the functional network template ( $T_{\text{inside}}$ ) and the mean *T*-value of all voxels outside the functional network template ( $T_{\text{outside}}$ ), i.e., goodness-of-fit =  $T_{\text{inside}} - T_{\text{outside}}$  [30]. A high goodness-of-fit score indicated a high correspondence of the pattern of correlated regions based on similar FDG uptake with certain network architecture. Due to the group-level nature of these analyses, no statistics were performed on the GOF scores. In order to test the robustness of the goodness-of-fit between the covariance maps and the functional network templates, these analyses were repeated with independent network templates from functional MRI data from 1000 healthy subjects from the Neurosynth project (<http://neurosynth.org> [31]). The templates were obtained by entering the MNI coordinates and downloading the generated functional networks. The templates were thresholded at a default threshold of  $r = 0.2$  using FSL to create binary masks.

### Metabolic connectivity—interaction analysis

In order to test statistical differences between patient groups in metabolic connectivity, we performed interaction analyses in SPM12. Differences between groups in metabolic connectivity were assessed in a key tAD network (i.e., DMN, with the posterior cingulate cortex as seed region [25]), and a key bvFTD network (i.e., the salience network, with the frontoinsula as seed region [39]). Multiple regressions were performed between the SUVR in the seed region and every other voxel in the brain, adding the SUVR within the seed region per group as a covariate, while adjusting for sex and age. Results were assessed both at  $p_{\text{uncorrected}} < 0.001$  and  $p_{\text{uncorrected}} < 0.05$ .

### Subcortical atrophy

We compared bvAD patients with tAD, bvFTD, and CN groups on gray matter volumes of several subcortical structures, including the amygdala, nucleus accumbens, caudate nucleus, putamen, globus pallidus, hippocampus, and thalamus. Volumes were extracted from T1-weighted MR scans, obtained at UCSF, either on a 1.5-T (Magnetom Avanto System/Magnetom VISION system, Siemens, Erlingen, Germany,  $n_{\text{bvAD}} = 17$ ) or 3-T (Tim Trio, Siemens, Erlingen, Germany,  $n_{\text{bvAD}} = 12$ ) all with a standard 12-channel head matrix coil. Acquisition parameters have been published previously [20]. Subcortical parcellations were performed using FSL FIRST [32]. First, the T1 images were transformed to MNI space using affine registration, and a subcortical mask was applied to the images. Next, subcortical structures were segmented bilaterally based on shape models and voxel intensities. All images were inspected visually after registration and segmentation. For each subcortical structure, left and right absolute volumes were generated, calculated in  $\text{cm}^3$ , and grouped together in the analysis, as there were no volume differences based on laterality. Statistical differences in volumes between groups were assessed using a general linear model, including all subcortical structures, with age, sex, scanner field strength, and total intracranial volume, which were obtained by summing the gray matter, white matter, and CSF volumes after segmentation in SPM12 [33], as covariates. Significant group differences were indicated by  $p < 0.05$ , Bonferroni corrected.

### White matter hyperintensity volumes

Next, we compared bvAD patients with tAD, bvFTD, and CN groups on white matter hyperintensity volumes (WMHV), using a Bayesian Model Selection (BaMoS) algorithm on FLAIR-MR images [34, 35]. Briefly, this method is a hierarchical, fully unsupervised model selection framework based on a Gaussian mixture model for neuroimaging data which enables the distinction between different types of abnormal image patterns without a

priori knowledge, accounting for observation outliers and incorporating anatomical priors. Lesion volumes were calculated for four equidistant concentric regions of white matter between the ventricles and cortices per lobe bilaterally [36]. All FLAIR-MR images were visually inspected prior to inclusion in the algorithm and those with significant motion or reconstruction artifacts were excluded, resulting in the exclusion of 1 bvAD patient, 2 tAD patients and 1 bvFTD patient. The WMHV segmentation was checked for quality and images with evident over- or underestimation were re-analyzed with an adjusted algorithm until satisfactory segmentation was obtained. Regional WMHV were normalized to the population of cognitively normal subjects, and statistical differences in WMHV between groups were assessed using a generalized linear model with gamma probability distribution and log link, adjusting for age, sex, scanner field strength, and total intracranial volume. Significant group differences were indicated by  $p < 0.05$ , and no correction for multiple comparisons was used due to the large correlation between dependent variables.

### Differentiating bvAD from tAD and bvFTD

To aid clinical differential diagnosis, receiver operating characteristic (ROC) analyses were performed to examine the area-under-the-curve (AUC) for discriminating bvAD from tAD and bvFTD. As input for the AUC analysis, we used various neuroimaging measures investigated in aim 1: measures of glucose metabolism, subcortical atrophy and white matter hyperintensities. For glucose metabolism, we extracted SUVR values from two AD-signature ROIs (i.e., temporoparietal cortex [37] and a total parietal ROI based on the Automated Anatomical Labeling (AAL) atlas regions [38]) and one FTD-signature ROI (comprising the anterior cingulate, frontoinsula, striatal and frontopolar AAL atlas regions [39, 40]). In addition, we extracted mean SUVR values within functional network templates as provided by Shirer et al. [29] and divided them by the SUVR values outside the network templates ( $\text{SUVR}_{\text{within network}}/\text{SUVR}_{\text{outside network}}$ ), thereby creating individual ratios of relative hypometabolism within networks. For subcortical structures, only the amygdala was added to the ROC analysis based on assessment of differences in subcortical volumes between diagnostic groups. For WMHV, weighted WMHV per lobe were included. Since we were interested in how the aim 1 neuroimaging measures related to structural MRI measures, we additionally used relevant structural MRI as input for the ROC analyses from the individuals that also had FDG-PET available. We extracted gray matter volumes from the same AD-signature and FTD-signature ROIs as used for glucose metabolism analyses. In addition, we created ratios of gray matter volumes within networks divided by gray matter volumes outside of network templates for all



networks included in the FDG-PET step. Pairwise ROC analyses between all groups were performed separately for all measures, as the sizes of the groups per modality varied. We present the top-5 best discriminatory variables in the main text and provide an overview of all results in Supplement 6.

**Results**

The patient groups did not differ in age, sex, and MMSE (Table 1). The level of education was higher in the cognitively normal group compared to each of the three patient groups ( $p < 0.01$ ), while there were no differences between the patient groups. The proportion of APOEε4 positive patients was higher in the bvAD and tAD groups compared to cognitively normal controls ( $p < 0.01$ ) and bvFTD patients ( $p < 0.001$ ). Cognitive and NPI scores are presented in Table 1. There were no substantial differences in demographic characteristics between the different subsets of patients that had FDG-PET, T1-MRI, or FLAIR-MRI available (see Supplement 2).

**Neuroimaging markers in bvAD**

**Glucose hypometabolism**

Compared to cognitively normal controls, marked hypometabolism was found in the posterior cingulate, precuneus, and lateral temporoparietal regions in both bvAD and tAD, while bvFTD displayed hypometabolism mainly in frontal regions and the temporal poles (Fig. 1a,

b). In direct patient group contrasts, bvAD showed no differences in glucose metabolism with tAD and less frontal hypometabolism than bvFTD ( $p < 0.001$ , uncorrected, see Supplement 7 for spatial patterns of patient vs. patient contrasts). Visual assessment of the overlay of *T*-maps resulting from voxel-wise comparisons between patients and cognitively normal controls suggested broader frontoinsula involvement in bvAD than in tAD, comprising the right lateral frontal lobe and bilateral insulae (Fig. 1c). Head-to-head comparison between FDG hypometabolic patterns with MRI atrophy patterns showed that the observed differences in the MR analysis were confined to a limited amount of regions (Supplement 8), while the differences were more pronounced on FDG-PET (Fig. 1).

**Metabolic connectivity—goodness-of-fit analysis**

bvAD patients showed a higher GOF score in the anterior DMN than tAD patients ( $GOF = 4.13$  versus  $2.92$ , respectively), which was identical to the bvFTD GOF score ( $4.13$ ). The GOF score for bvAD ( $3.85$ ) in the posterior DMN was intermediate between bvFTD ( $2.04$ ) and tAD ( $4.14$ ), but closer to tAD. In the salience network, bvFTD had a higher GOF score ( $2.90$ ) than both tAD ( $0.62$ ) and bvAD ( $1.05$ ). In the executive control network, bvAD patients ( $2.20$ ) showed a lower GOF score than tAD ( $3.11$ ) and bvFTD ( $2.78$ ) patients (Fig. 2 & Supplement 3). Sensitivity analyses using

**Table 1** Participant characteristics

	<b>bvAD</b>	<b>tAD</b>	<b>bvFTD</b>	<b>CN<sub>1</sub></b>	<b>p value</b>
<i>n</i>	29	28	28	34	
Age, years	64.4 (9.4)	63.0 (9.3)	64.6 (4.4)	64.9 (9.9)	0.84
Sex, no. male (%)	17 (59)	16 (55)	21 (70)	22 (65)	0.82
Education <sup>a</sup> , years mean (SD)	15.7 (2.6)	15.8 (2.8)	15.1 (3.4)	17.9 (2.0)	0.001
MMSE <sup>b</sup> †, mean (SD)	22.0 (5.9)	22.1 (5.7)	21.3 (6.7)	29.5 (0.7)	0.001
APOEε4 positivity <sup>c</sup> , no. of patients (%)	11/18 (61)	10/14 (67)	3/27 (11)	6/34 (18)	< 0.001
MRI scanner field strength					0.16
1.5 T	17 (59)	22 (79)	14 (50)	22 (65)	
3 T	12 (41)	6 (21)	14 (50)	12 (35)	
Memory domain z-score <sup>d</sup> °, mean (SD)	− 3.5 (1.5)	− 3.9 (1.3)	− 2.8 (1.7)	0.3 (0.9)	< 0.001
Executive domain z-score <sup>e</sup> °, mean (SD)	− 1.9 (1.0)	− 1.9 (1.0)	− 2.1 (1.0)	0.0 (0.6)	< 0.001
NPI score <sup>f</sup> °, mean (SD)	30.2 (20.6)	12.8 (15.4)	34.7 (17.2)	–	0.001

Differences between groups were assessed using (M)ANOVA tests, chi-square tests, and Kruskal-Wallis tests with post hoc Mann-Whitney *U* tests, where appropriate. All *p* values were corrected for multiple comparisons using Bonferroni correction. Data presented above are based on the groups for whom T1 MRI scans were available. See Supplement 2 for equivalent information in groups for which FDG and FLAIR-MRI scans were available

†MMSE data was available for *n* = 26 for bvAD, *n* = 19 for tAD, *n* = 27 for bvFTD, and *n* = 34 for CN<sub>1</sub>

°Cognition data was available for *n* = 22 for bvAD, *n* = 28 for tAD, *n* = 24 for bvFTD, and *n* = 30 for CN<sub>1</sub>

°NPI data was available for *n* = 13 for bvAD, *n* = 18 for tAD, *n* = 20 for bvFTD, and *n* = 0 for CN<sub>1</sub>

<sup>a</sup>Controls > patients,  $p < 0.01$

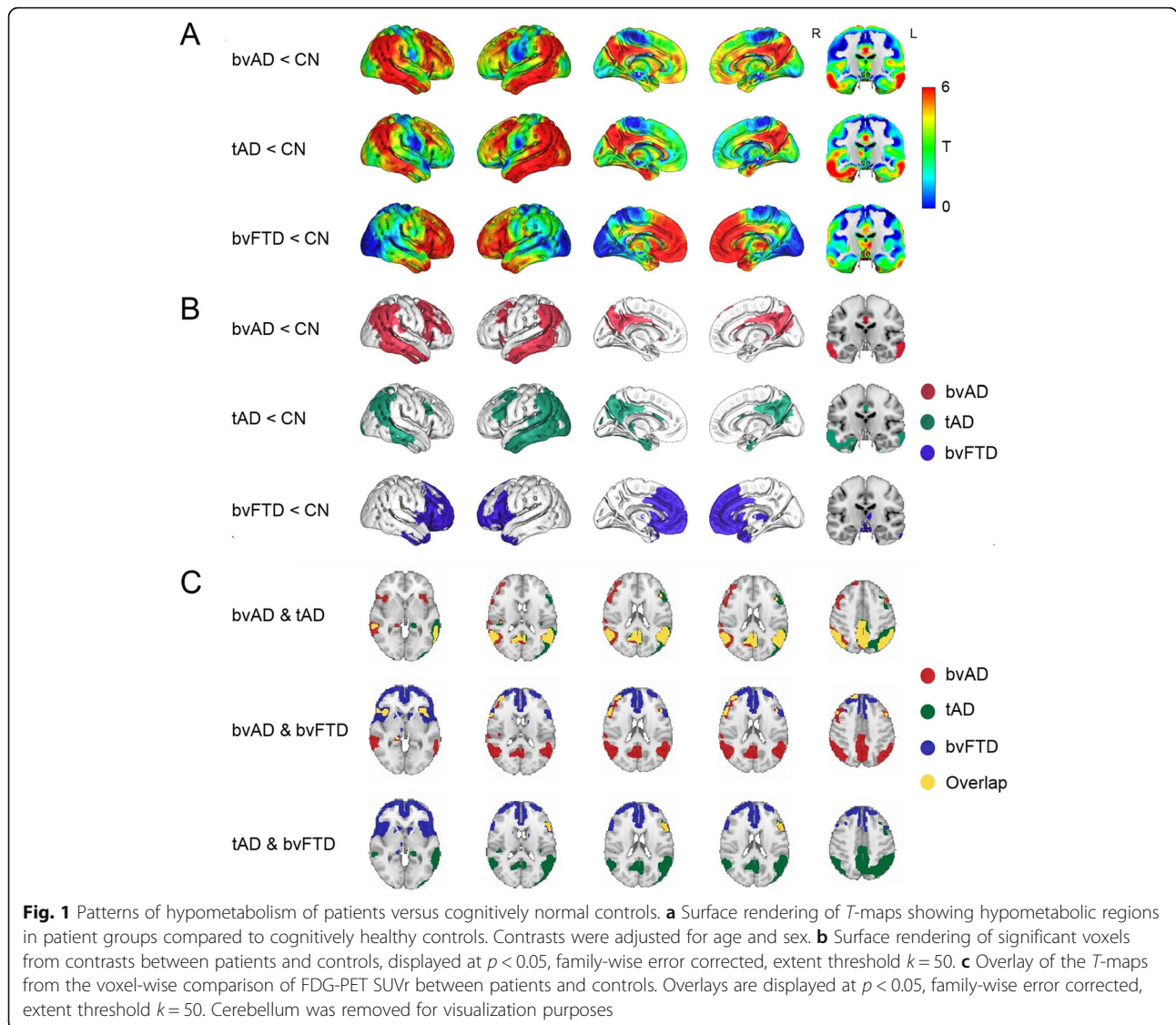
<sup>b</sup>Controls > patients,  $p < 0.001$

<sup>c</sup>bvAD and tAD > controls,  $p < 0.01$ , bvAD and tAD > bvFTD,  $p < 0.001$

<sup>d</sup>Controls > patients,  $p < 0.001$ , tAD < bvFTD,  $p < 0.05$

<sup>e</sup>Controls > patients,  $p < 0.001$

<sup>f</sup>bvAD and bvFTD > tAD,  $p < 0.01$



different functional network templates showed a similar pattern of GOF scores (Supplement 3).

**Metabolic connectivity—interaction analysis**

The interaction analysis showed significantly less metabolic connectivity of the PCC with (right) prefrontal regions in bvAD compared to tAD (Fig. 2b) and more connectivity to (left) temporal and occipital regions in bvAD than tAD. Differences in connectivity of the frontoinsula to the rest of the cortex were marginal between bvAD and tAD patients (Fig. 2b). bvAD and tAD patients both showed more connectivity of the frontoinsula to anterior regions and less connectivity to posterior regions compared to bvFTD patients, showing similar patterns in these comparisons. Supplement 4 summarizes the most significant clusters of altered metabolic connectivity.

**Subcortical atrophy**

Compared to cognitively normal controls, bvAD showed lower gray matter volumes in the hippocampus, putamen, caudate nucleus, and thalamus, and no significant differences in the amygdala, nucleus accumbens, and globus pallidus, while tAD patients showed lower volumes in the hippocampus, amygdala, nucleus accumbens, and thalamus and bvFTD patients showed lower volumes in all subcortical structures compared to cognitively normal controls. bvAD showed larger amygdala gray matter volume than tAD ( $p < 0.05$ ) and no differences with tAD in all other examined structures. In comparison with bvFTD, bvAD and tAD patients showed larger globus pallidus gray matter volumes ( $p < 0.05$ ), tAD patients showed larger nucleus accumbens gray matter volumes ( $p < 0.05$ ), and no differences with bvAD were found in other structures (Fig. 3 and Supplement 5).

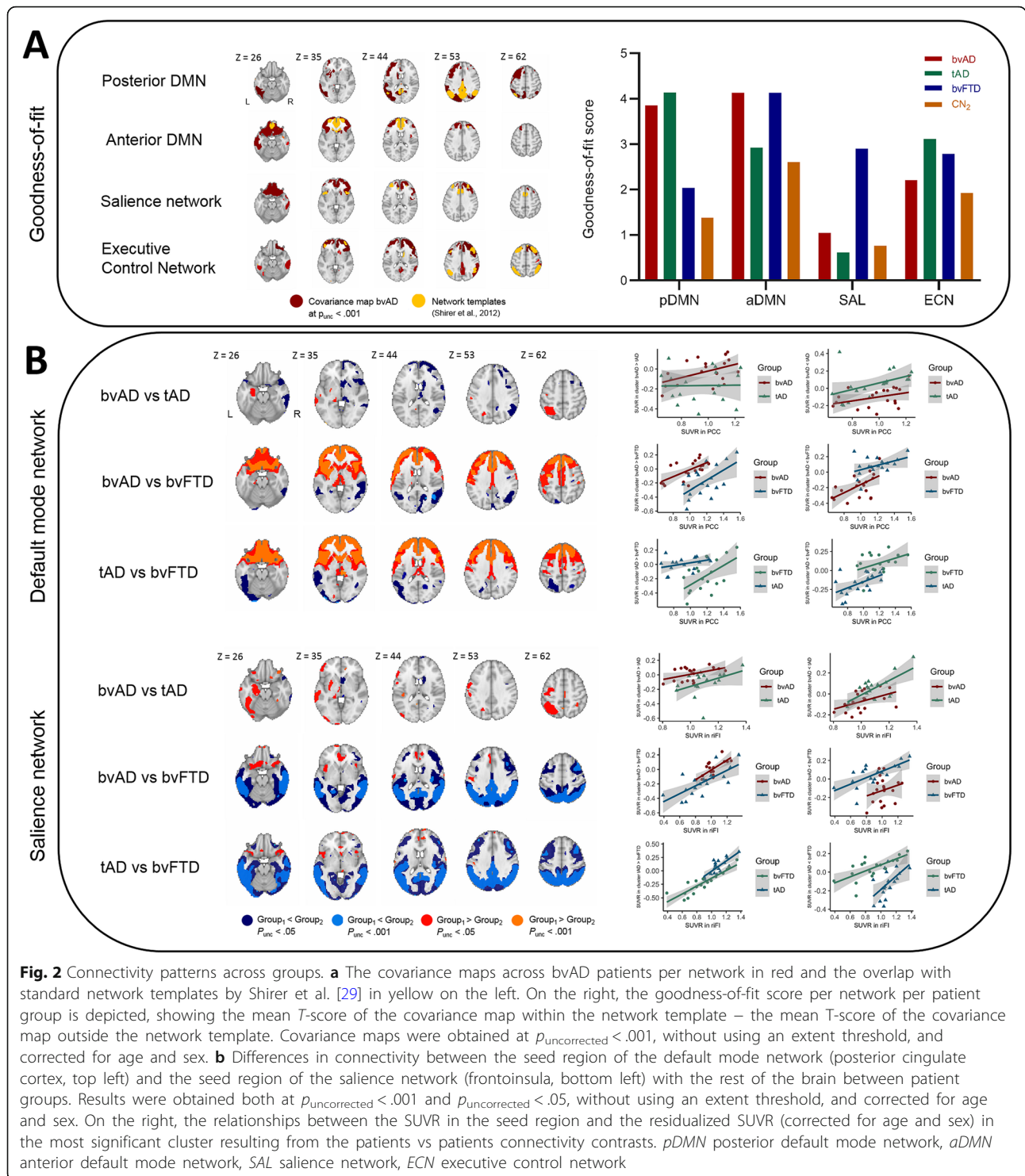


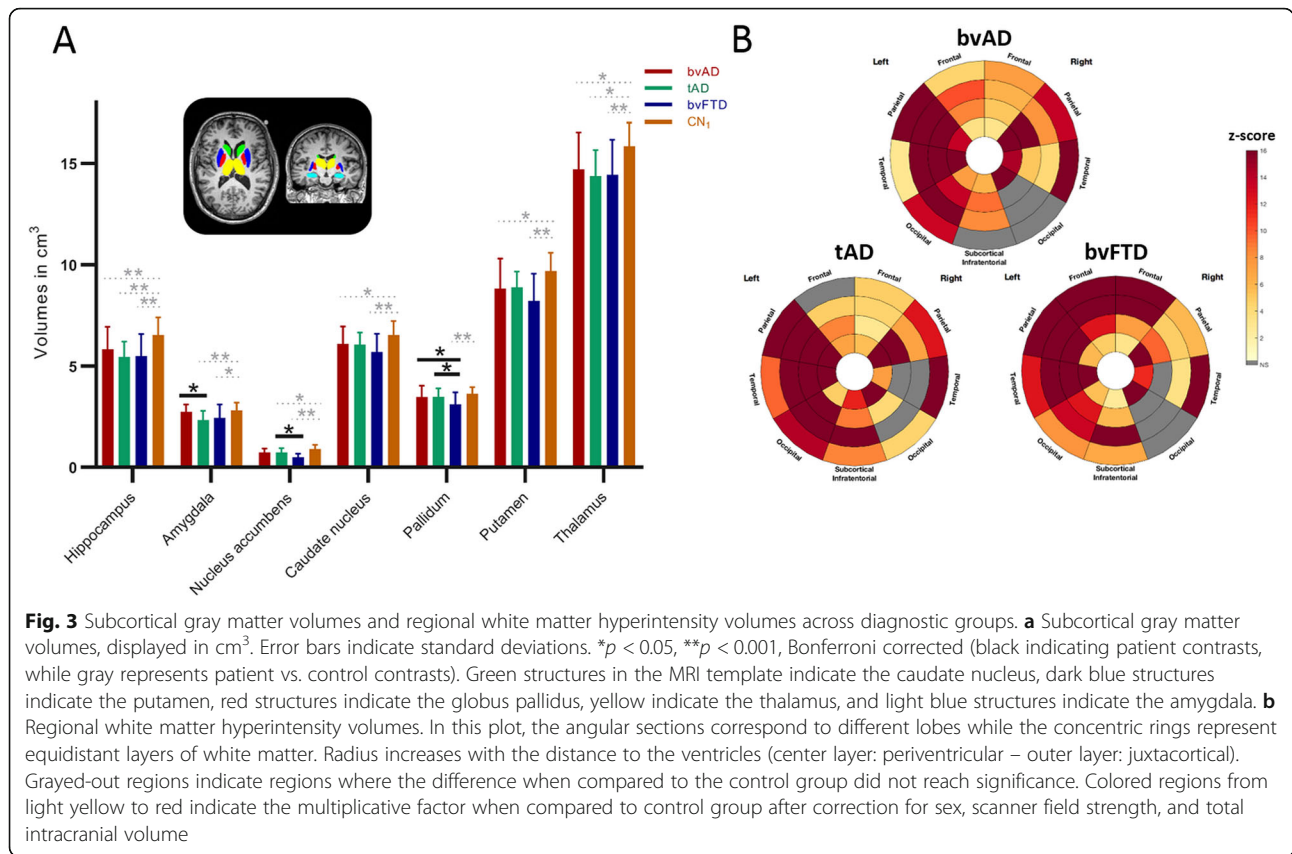
**Fig. 2** Connectivity patterns across groups. **a** The covariance maps across bvAD patients per network in red and the overlap with standard network templates by Shirer et al. [29] in yellow on the left. On the right, the goodness-of-fit score per network per patient group is depicted, showing the mean  $T$ -score of the covariance map within the network template – the mean  $T$ -score of the covariance map outside the network template. Covariance maps were obtained at  $p_{uncorrected} < .001$ , without using an extent threshold, and corrected for age and sex. **b** Differences in connectivity between the seed region of the default mode network (posterior cingulate cortex, top left) and the seed region of the saliency network (frontoinsula, bottom left) with the rest of the brain between patient groups. Results were obtained both at  $p_{uncorrected} < .001$  and  $p_{uncorrected} < .05$ , without using an extent threshold, and corrected for age and sex. On the right, the relationships between the SUVR in the seed region and the residualized SUVR (corrected for age and sex) in the most significant cluster resulting from the patients vs patients connectivity contrasts. *pDMN* posterior default mode network, *aDMN* anterior default mode network, *SAL* saliency network, *ECN* executive control network

**White matter hyperintensities**

No differences were found between the patient groups in total WMHV, nor were regional differences found in WMHV between the patient groups (all  $p > 0.05$ , Supplement 5). Controls showed less WMHV in the basal ganglia and infratentorial regions than bvAD

and bvFTD ( $p < 0.01$ , Supplement 5), but no differences with patient groups in other regions. Sub-regional analysis revealed lower frontal juxtacortical WMHV in bvAD than bvFTD, as well as lower left temporal juxtacortical WMHV, and higher right temporal juxtacortical WMHV ( $p < 0.05$ , Fig. 4). In





comparison to tAD, bvAD patients showed lower juxtacortical left temporal and subcortical WMHV and higher right temporal juxtacortical WMHV (*p* < 0.05, Fig. 3b).

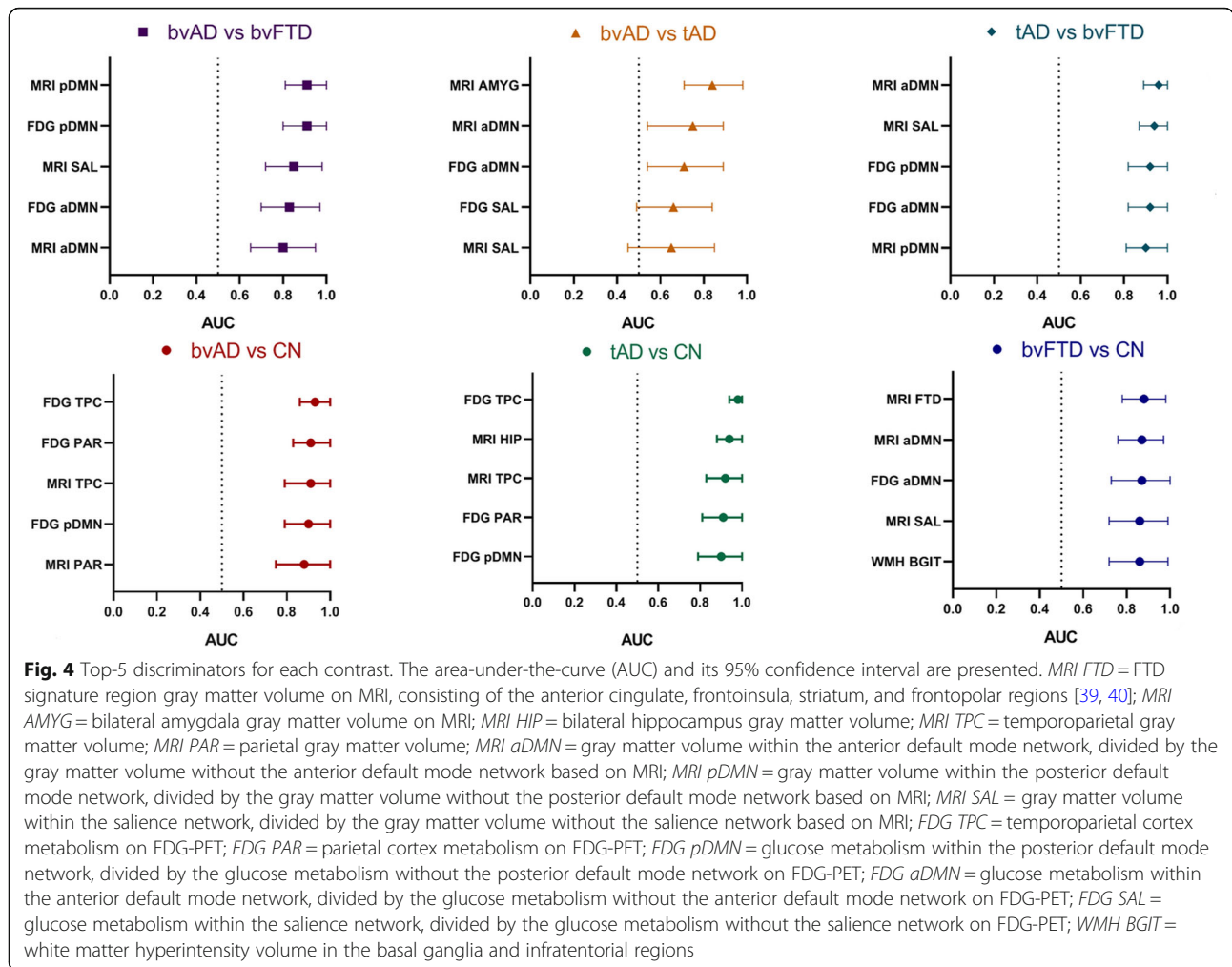
### Differentiating bvAD from tAD and bvFTD

A summary of all measures is included in Supplement 6. The top-5 discriminative variables for bvAD vs. bvFTD were MRI posterior DMN ratios (bvAD<bvFTD; AUC = 0.91 [95%CI = 0.81–1.00]), FDG posterior DMN ratios (bvAD<bvFTD; AUC = 0.91 [0.80–1.00]), MRI salience network ratios (bvAD>bvFTD, AUC = 0.85 [0.72–0.98]), FDG anterior DMN ratios (bvAD>bvFTD, AUC = 0.83 [0.70–0.97]), and MRI anterior DMN ratios (bvAD>bvFTD, AUC = 0.80 [0.65–0.95]) (Fig. 4 and Supplement 6). bvAD was discriminated best from tAD by amygdalar volume (bvAD>tAD; AUC = 0.84 [95%CI = 0.71–0.98]), MRI anterior DMN ratios (bvAD<tAD, AUC = 0.75 [0.59–0.92]), FDG anterior DMN ratios (bvAD<tAD, AUC = 0.71 [0.54–0.89]), FDG salience network ratios (bvAD<tAD, AUC = 0.66 [0.49–0.84]), and MRI salience network ratios (bvAD<tAD, AUC = 0.65 [0.45–0.85]). The top-5 discriminative variables for bvAD vs. CN were temporoparietal hypometabolism (AUC = 0.93 [0.86–1.00]), parietal hypometabolism (AUC = 0.91 [0.83–1.00]), temporoparietal atrophy (AUC = 0.91 [0.83–0.99]), hypometabolism in the posterior DMN

(AUC = 0.90 [0.79–1.00]), and parietal atrophy (AUC = 0.89 [0.79–0.99]).

### Discussion

The aims of the current study were (i) to explore the clinico-anatomical dissociation observed in bvAD (i.e., relative lack of frontal atrophy with prominent behavioral changes [1]) through assessment of multiple imaging markers and (ii) to examine the diagnostic accuracy of several neuroimaging measures for differentiating bvAD from tAD and bvFTD. We hypothesized that bvAD patients would exhibit more anterior hypometabolism, more pronounced alterations of metabolic connectivity networks involved in behavioral processes, greater subcortical atrophy, and a greater white matter hyperintensity burden in regions impacting frontosubcortical tracts compared to tAD, and would partly resemble the neuroimaging characteristics of bvFTD. Our results suggest that the behavioral symptoms presented by bvAD patients are associated with subtle fronto-insular hypometabolism, increased anterior default mode involvement, and reduced connectivity of the posterior cingulate cortex to the right prefrontal cortex. In addition, our results suggest that subcortical atrophy and white matter hyperintensities may not play a major role in the clinical phenotype of bvAD. The ROC analyses showed that ratios of both hypometabolism and atrophy within networks



versus the signal outside the network templates were strong discriminators between diagnostic groups, and amygdalar gray matter volume was the strongest discriminator between bvAD and tAD. The pattern of hypometabolism in bvAD points towards subtle loss of neural activity in fronto-insular regions in addition to posterior “AD-typical” regions. This represents a variant-specific pattern of hypometabolism in addition to a common involvement of temporoparietal cortex across amnesic and non-amnesic variants of AD [20, 41, 42]. This suggests that either the disease epicenter may differ between these AD variants, or that neurodegeneration spreads faster into fronto-insular regions in bvAD compared to tAD, where the frontal regions typically stay spared until more advanced disease stages. As FDG-PET has been suggested to capture the same underlying mechanisms with higher sensitivity than MRI [43], the overlap of temporoparietal hypometabolic pattern with the atrophy pattern and additional involvement of fronto-insular hypometabolism suggests FDG-PET may capture early spread of neurodegeneration into fronto-insular regions in bvAD. Our findings in a clinically defined group of bvAD

patients are in line with a FDG-PET study showing reduced frontal hypometabolism in AD patients with pronounced neuropsychiatric symptoms as indicated by a behavioral questionnaire [44]. However, as MRI measures came out as strong discriminators in addition to FDG-PET measures, the clinical utility of MRI in the differential diagnosis of bvAD should not be underestimated. The involvement of the anterior DMN as well as the posterior DMN in bvAD patients provides insights into their clinical presentation, as the anterior DMN is associated with social cognitive functions, such as affective self-referential processing and the inference of other’s mental state [25, 45], whereas the posterior DMN has been related to several cognitive processes including temporal episodic memory and thinking about the future [25, 46]. bvAD patients resembled tAD patients in the involvement of posterior DMN (reflecting their shared underlying AD pathology or cognitive profile), while bvAD patients showed equivalent involvement of the anterior DMN as bvFTD patients (reflecting their shared behavioral phenotype). In addition, bvAD patients showed significantly reduced connectivity between the PCC and the

right prefrontal cortex compared to typical AD patients in a voxelwise interaction analysis. On structural MRI, no subcortical region showed greater atrophy in bvAD compared to tAD and bvFTD, and the regional WMHV profiles showed more similarities with tAD than with bvFTD. The only deep gray matter structure that showed differences between bvAD and tAD was the amygdala, which showed larger volumes in patients with bvAD than tAD. Although speculative, based on the fact that bvAD did not differ from cognitively normal controls, this could represent larger pre-morbid amygdalar volumes in bvAD at baseline, which, with the same rate of atrophy, progress to the same volumes as cognitively normal controls, as larger amygdalae have been reported in several neuropsychiatric disorders, such as depression [47] and autism [48]. Alternatively, the amygdala may fall further downstream from the pathophysiological epicenter in bvAD and remain more preserved than in tAD. Due to its central role in fear processing and responsivity to emotionally salient stimuli, this structure may be of importance to the clinical phenotype of bvAD. These hypotheses should be investigated in future studies, preferentially with a longitudinal design. The ROC analyses showed that relative hypometabolism or atrophy within network templates may aid the differentiation of bvAD from tAD and bvFTD. These results could improve clinical practice by suggesting assessment of relative atrophy or hypometabolism within network templates in addition to traditional regions. In addition to neuroimaging markers, there is a need for improving clinical diagnostic tools. As the assessment of presence of behavioral abnormalities currently largely depend on subjective ratings of either clinicians or caregivers, future studies should focus on exploring more objective ways to measure behavioral disturbances, e.g., social cognition test batteries or validated questionnaires in order to improve diagnostic accuracy.

It should be noted that in this study, only patients with behavioral-predominant presentations were included, while patients with isolated dysexecutive deficits were not. It has been under debate whether these presentations represent separate clinical entities or whether they represent different aspects of a single continuum [1]. Since we found only a modest overlap between the groups (9/75, 12%) in our previous work [1], the recently proposed research criteria for dysexecutive AD do not include the behavioral phenotype [49], and behavior and executive functioning may be conceptually as well as neurobiologically distinct processes [24], we chose not to include dysexecutive presentations in the absence of behavioral dysfunction.

### Strengths and limitations

Strengths of the current study include the relatively large sample of clinically defined bvAD patients with multiple neuroimaging markers available. This allowed for a

comprehensive examination of neurobiological features and the clinical utility of a broad range of diagnostic tools in this relatively rare variant of AD. The results of the present study also need to be viewed in light of some limitations. First and foremost, data availability across imaging modalities varied. Although we showed that the ROC analyses yielded largely the same results when performed in patients with both MRI and FDG-PET available as compared to the whole group with MRI available, this is a major limitation that is inherent to the retrospective nature of the study as well as the unstandardized data collection. Other limitations include the lack of fMRI data in this group to study functional connectivity, and future studies should investigate the dysexecutive variant of AD in addition to bvAD. Moreover, there is a possibility of circularity in the FDG-PET results as patients with anterior hypometabolism may be diagnosed with bvFTD, despite our strict inclusion procedure that required all bvAD patients to be amyloid-positive and all bvFTD patients to be amyloid-negative. Lastly, our typical AD group consisted of relatively young patients. As an early age-at-onset is associated with a more anterior distribution of neurodegeneration [20], this may decrease the probability of observing group differences with bvAD. However, since the typical AD group included in this study showed a predominant temporoparietal pattern compared to healthy controls, these effects are likely marginal.

### Conclusions

Overall, somewhat contrary to our hypotheses, bvAD patients showed greater overlap of neuroimaging features with tAD than with bvFTD, further emphasizing their classification as AD patients as opposed to FTD patients with comorbid amyloid pathology [10]. In addition, these results confirm the notion that the term “frontal AD” is not an appropriate description of this phenotype and instead re-emphasize the usage of the term “behavioral variant of AD” [1]. Our results show that the differentiation of bvAD from typical AD may lie in subtle differences in frontoinsular metabolism, altered connectivity of the anterior default mode network, differential amygdalar neurodegeneration and relative hypometabolism or atrophy in the default mode network compared to other regions, which may explain, to some extent, the prominent behavioral presentation in bvAD. However, future studies should investigate other potential neurobiological factors, such as distribution of tau pathology and involvement of other pathological mechanisms such as decreased Von Economo Neuron [50] density in the anterior cingulate cortex (associated with social behavior), as well as premorbid personality traits and social cognition in a prospective cohort of bvAD patients, in order to understand the peculiar behavioral presentation

in this AD variant that seems to hold relatively little reference to our existing conception of clinico-anatomical relationships.

### Supplementary information

Supplementary information accompanies this paper at <https://doi.org/10.1186/s13195-020-00717-z>.

**Additional file 1 : Supplement 1.** Data availability per modality.

**Additional file 2 : Supplement 2.** Participant characteristics of subgroups.

**Additional file 3 : Supplement 3.** Goodness-of-fit scores of networks.

**Additional file 4 : Supplement 4.** Clusters in SPM interaction analysis.

**Additional file 5 : Supplement 5.** Subcortical and white matter volume.

**Additional file 6 : Supplement 6.** Receiver-operating-characteristics analysis.

**Additional file 7 : Supplement 7.** Hypometabolism between patients contrasts.

**Additional file 8 : Supplement 8.** Grey matter atrophy.

### Abbreviations

AD: Alzheimer's disease; A $\beta$ :  $\beta$ -Amyloid; bvAD: Behavioral variant of Alzheimer's disease; bvFTD: Behavioral variant of frontotemporal dementia; MCI: Mild cognitive impairment; MMSE: Mini-Mental State Examination; UCSF: University of California San Francisco; MRI: Magnetic resonance imaging

### Acknowledgements

We are grateful to all participants for their time and effort. In addition, the authors would like to acknowledge Gemma Salvadó for her help with the conduction of the connectivity SPM interaction analysis.

### Publication history

This manuscript was previously published as a pre-print on the medRxiv website; MS ID#: MEDRXIV/2019/006676.

### Financial disclosures

Gil D. Rabinovici reports research support from Avid Radiopharmaceuticals, GE Healthcare, Eli Lilly, Life Molecular Imaging; Scientific advisory boards for Axon Neurosciences, Eisai, Merck, Roche; Associate Editor for JAMA Neurology. Frederik Barkhof reports research support from GE Healthcare, Biogen, Novartis, and TEVA; Scientific advisory boards for Roche, Biogen, Merck, Roche, Lundbeck and IXICO. Philip Scheltens serves/has served on the advisory boards of Genentech, Novartis, Pfizer, Roche, Danone, Nutricia, Jansen AI, Baxter, and Lundbeck. He has been a speaker at symposia organized by Lundbeck, Lilly, Merz, Pfizer, Jansen AI, Danone, Novartis, Roche, and Genentech. He serves on the editorial board of *Alzheimer's Research & Therapy* and *Alzheimer Disease and Associated Disorders* and is a member of the scientific advisory board of the EU Joint Programming Initiative and the French National Plan Alzheimer. The Alzheimer Center receives unrestricted funding from various sources through the VUmc Fonds. Dr. Scheltens receives no personal compensation for the activities mentioned above.

### Authors' contributions

ES: Study design, statistical analysis, analysis of imaging data, interpretation of data, and writing and revising the manuscript. YAL: Study design, interpretation of data, and revising the manuscript. CHS: Study design, imaging analyses, interpretation of data, and revising the manuscript. CG: Imaging analyses, interpretation of data, and revising the manuscript. EK: Imaging analyses, interpretation of data, and contributing to writing the manuscript. FB: Critical revision of manuscript for intellectual content. RLJ: Acquisition of patient data from UCSF, study design, imaging analyses, interpretation of data, and revising the manuscript. HJR: Critical revision of manuscript for intellectual content. WWS: Critical revision of manuscript for

intellectual content. BM: Critical revision of manuscript for intellectual content. JC: Critical revision of manuscript for intellectual content. JP: Critical revision of manuscript for intellectual content. PS: Acquisition of patient data from ADC, interpretation of results, and critical revision of manuscript for intellectual content. GDR: Acquisition of patient data from UCSF, interpretation of results, and critical revision of manuscript for intellectual content. RO: Study concept and design, statistical analysis, analysis of imaging data, writing and revising the manuscript, and supervised the study. The authors read and approved the final manuscript.

### Funding

Work at the Alzheimer Center Amsterdam was supported by the Netherlands Organisation for Health Research and Development, ZonMw (70-73305-98-1214 to Rik Ossenkoppele, PI). Research of the Alzheimer center Amsterdam is part of the neurodegeneration research program of Amsterdam Neuroscience. The Alzheimer Center Amsterdam is supported by Stichting Alzheimer Nederland and Stichting VUmc fonds. Work at the University of California San Francisco was supported by the NIH National Institute on Aging (NIA) grants R01-AG045611 (to G.D.R.).

### Availability of data and materials

Anonymized data used in the present study may be available upon request to the corresponding author.

### Ethics approval and consent to participate

Informed consent was obtained from all subjects or their assigned surrogate decision-makers, and the study was approved by the University of California Berkeley, UCSF, and Lawrence Berkeley National Laboratory institutional human research review boards.

### Consent for publication

Not applicable.

### Competing interests

The authors declare that they have no competing interests.

### Author details

<sup>1</sup>Alzheimer Center Amsterdam, Department of Neurology, Amsterdam Neuroscience, Vrije Universiteit Amsterdam, Amsterdam UMC, Amsterdam, the Netherlands. <sup>2</sup>School of Biomedical Engineering and Imaging Sciences, King's College London, London, UK. <sup>3</sup>Department of Radiology and Nuclear Medicine, Vrije Universiteit Amsterdam, Amsterdam UMC, Amsterdam, the Netherlands. <sup>4</sup>Center for Medical Image Computing, Department of Medical Physics and Biomedical Engineering, University College London, London, UK. <sup>5</sup>Department of Neurology, Memory and Aging Center, University of California San Francisco, San Francisco, USA. <sup>6</sup>Translational Imaging Group, CMIC, Department of Medical Physics and Biomedical Engineering, University College London, London, UK. <sup>7</sup>Department of Neurology, Erasmus University Medical Center, Rotterdam, the Netherlands. <sup>8</sup>Department of Radiology, Erasmus University Medical Center, Rotterdam, the Netherlands. <sup>9</sup>Department of Radiology and Biomedical Imaging, University of California San Francisco, San Francisco, USA. <sup>10</sup>Molecular Biophysics and Integrated Bioimaging Division, Lawrence Berkeley National Laboratory, Berkeley, CA, USA. <sup>11</sup>Helen Wills Neuroscience Institute, University of California Berkeley, Berkeley, USA. <sup>12</sup>Clinical Memory Research Unit, Lund University, Lund, Sweden.

Received: 4 August 2020 Accepted: 26 October 2020

Published online: 14 November 2020

### References

- Ossenkoppele R, Pijnenburg YA, Perry DC, Cohn-Sheehy BI, Scheltens NM, Vogel JW, et al. The behavioural/dysexecutive variant of Alzheimer's disease: clinical, neuroimaging and pathological features. *Brain*. 2015;138(Pt 9):2732–49.
- Blennerhassett R, Lillo P, Halliday GM, Hodges JR, Kril JJ. Distribution of pathology in frontal variant Alzheimer's disease. *J Alzheimer's Dis*. 2014;39(1):63–70.
- Kawakatsu S, Kobayashi R, Hayashi H. Typical and atypical appearance of early-onset Alzheimer's disease: a clinical, neuroimaging and neuropathological study. *Neuropathol*. 2017;37(2):150–73.
- Phillips JS, Da Re F, Dratch L, Xie SX, Irwin DJ, McMillan CT, et al. Neocortical origin and progression of gray matter atrophy in nonamnestic Alzheimer's disease. *Neurobiol Aging*. 2018;63:75–87.



5. Wong S, Strudwick J, Devenney E, Hodges JR, Piguet O, Kumfor F. Frontal variant of Alzheimer's disease masquerading as behavioural-variant frontotemporal dementia: a case study comparison. *Neurocase*. 2019;25(1–2):48–58.
6. Chetelat G, Desgranges B, Landeau B, Mezenge F, Poline JB, de la Sayette V, et al. Direct voxel-based comparison between grey matter hypometabolism and atrophy in Alzheimer's disease. *Brain*. 2008;131(Pt 1):60–71.
7. Lee DS, Kang H, Kim H, Park H, Oh JS, Lee JS, et al. Metabolic connectivity by interregional correlation analysis using statistical parametric mapping (SPM) and FDG brain PET; methodological development and patterns of metabolic connectivity in adults. *Eur J Nucl Med Mol Imaging*. 2008;35(9):1681–91.
8. Reed BR, Eberling JL, Mungas D, Weiner M, Kramer JH, Jagust WJ. Effects of white matter lesions and lacunes on cortical function. *Arch Neurol*. 2004;61(10):1545–50.
9. Tekin S, Cummings JL. Frontal-subcortical neuronal circuits and clinical neuropsychiatry: an update. *J Psychosom Res*. 2002;53(2):647–54.
10. Scialo C, Ferrara M, Accardo J, Morbelli S, Picco A, Arnaldi D, et al. Frontal variant Alzheimer disease or frontotemporal lobe degeneration with incidental amyloidosis? *Alzheimer Dis Assoc Disord*. 2016;30(2):183–5.
11. McKhann GM, Knopman DS, Chertkow H, Hyman BT, Jack CR Jr, Kawas CH, et al. The diagnosis of dementia due to Alzheimer's disease: recommendations from the National Institute on Aging-Alzheimer's Association workgroups on diagnostic guidelines for Alzheimer's disease. *Alzheimer's Dement*. 2011;7(3):263–9.
12. Albert MS, DeKosky ST, Dickson D, Dubois B, Feldman HH, Fox NC, et al. The diagnosis of mild cognitive impairment due to Alzheimer's disease: recommendations from the National Institute on Aging-Alzheimer's Association workgroups on diagnostic guidelines for Alzheimer's disease. *Alzheimer's Dement*. 2011;7(3):270–9.
13. Neary D, Snowden JS, Gustafson L, Passant U, Stuss D, Black S, et al. Frontotemporal lobar degeneration: a consensus on clinical diagnostic criteria. *Neurology*. 1998;51(6):1546–54.
14. Rascoy K, Hodges JR, Knopman D, Mendez MF, Kramer JH, Neuhaus J, et al. Sensitivity of revised diagnostic criteria for the behavioural variant of frontotemporal dementia. *Brain*. 2011;134(Pt 9):2456–77.
15. Mormino EC, Kluth JT, Madison CM, Rabinovici GD, Baker SL, Miller BL, et al. Episodic memory loss is related to hippocampal-mediated beta-amyloid deposition in elderly subjects. *Brain*. 2009;132(Pt 5):1310–23.
16. Ossenkoppele R, Madison C, Oh H, Wirth M, van Berckel BN, Jagust WJ. Is verbal episodic memory in elderly with amyloid deposits preserved through altered neuronal function? *Cerebral Cortex (New York)*. 2014;24(8):2210–8.
17. Minoshima S, Frey KA, Foster NL, Kuhl DE. Preserved pontine glucose metabolism in Alzheimer disease: a reference region for functional brain image (PET) analysis. *J Comput Assist Tomogr*. 1995;19(4):541–7.
18. Ossenkoppele R, van der Flier WM, Verfaillie SC, Vrenken H, Versteeg A, van Schijndel RA, et al. Long-term effects of amyloid, hypometabolism, and atrophy on neuropsychological functions. *Neurology*. 2014;82(20):1768–75.
19. Yakushev I, Drzezga A, Habeck C. Metabolic connectivity: methods and applications. *Curr Opin Neurol*. 2017;30(6):677–85.
20. Lehmann M, Ghosh PM, Madison C, Laforce R Jr, Corbetta-Rastelli C, Weiner MW, et al. Diverging patterns of amyloid deposition and hypometabolism in clinical variants of probable Alzheimer's disease. *Brain*. 2013;136(Pt 3):844–58.
21. Zhou J, Greicius MD, Gennatas ED, Growdon ME, Jang JY, Rabinovici GD, et al. Divergent network connectivity changes in behavioural variant frontotemporal dementia and Alzheimer's disease. *Brain*. 2010;133(Pt 5):1352–67.
22. Raichle ME. The brain's default mode network. *Annu Rev Neurosci*. 2015;38:433–47.
23. Menon V, Uddin LQ. Saliency, switching, attention and control: a network model of insula function. *Brain Struct Funct*. 2010;214(5–6):655–67.
24. Seeley WW, Menon V, Schatzberg AF, Keller J, Glover GH, Kenna H, et al. Dissociable intrinsic connectivity networks for salience processing and executive control. *J Neurosci*. 2007;27(9):2349–56.
25. Andrews-Hanna JR, Reidler JS, Sepulcre J, Poulin R, Buckner RL. Functional-anatomic fractionation of the brain's default network. *Neuron*. 2010;65(4):550–62.
26. Leech R, Kamourieh S, Beckmann CF, Sharp DJ. Fractionating the default mode network: distinct contributions of the ventral and dorsal posterior cingulate cortex to cognitive control. *J Neurosci*. 2011;31(9):3217–24.
27. Uddin LQ, Kelly AM, Biswal BB, Castellanos FX, Milham MP. Functional connectivity of default mode network components: correlation, anticorrelation, and causality. *Hum Brain Mapp*. 2009;30(2):625–37.
28. Menon V. Salience Network. In: Arthur W. Toga, editor. *Brain Mapping: An Encyclopedic Reference*, 2015. vol. 2, pp. 597–611. Academic Press: Elsevier.
29. Shirer WR, Ryali S, Rykhlevskaia E, Menon V, Greicius MD. Decoding subject-driven cognitive states with whole-brain connectivity patterns. *Cerebral Cortex (New York)*. 2012;22(1):158–65.
30. Ossenkoppele R, Iaccarino L, Schonhaut DR, Brown JA, La Joie R, O'Neil JP, et al. Tau covariance patterns in Alzheimer's disease patients match intrinsic connectivity networks in the healthy brain. *NeuroImage Clin*. 2019;23:101848.
31. Yarkoni T, Poldrack RA, Nichols TE, Van Essen DC, Wager TD. Large-scale automated synthesis of human functional neuroimaging data. *Nat Methods*. 2011;8(8):665–70.
32. Patenaude B, Smith SM, Kennedy DN, Jenkinson M. A Bayesian model of shape and appearance for subcortical brain segmentation. *NeuroImage*. 2011;56(3):907–22.
33. Malone IB, Leung KK, Clegg S, Barnes J, Whitwell JL, Ashburner J, et al. Accurate automatic estimation of total intracranial volume: a nuisance variable with less nuisance. *NeuroImage*. 2015;104:366–72.
34. Sudre CH, Cardoso MJ, Bouvy WH, Biessels GJ, Barnes J, Ourselin S. Bayesian model selection for pathological neuroimaging data applied to white matter lesion segmentation. *IEEE Trans Med Imaging*. 2015;34(10):2079–102.
35. Groot C, Sudre CH, Barkhof F, Teunissen CE, van Berckel BNM, Seo SW, et al. Clinical phenotype, atrophy, and small vessel disease in APOEepsilon2 carriers with Alzheimer disease. *Neurology*. 2018;91(20):e1851–e9.
36. Sudre CH, Gomez Anson B, Davagnanam I, Schmitt A, Mendelson AF, Prados F, et al. Bullseye's representation of cerebral white matter hyperintensities. *J Neuroradiol*. 2018;45(2):114–22.
37. Ossenkoppele R, Cohn-Sheehy BI, La Joie R, Vogel JW, Moller C, Lehmann M, et al. Atrophy patterns in early clinical stages across distinct phenotypes of Alzheimer's disease. *Hum Brain Mapp*. 2015;36(11):4421–37.
38. Tzourio-Mazoyer N, Landeau B, Papathanassiou D, Crivello F, Etard O, Delcroix N, et al. Automated anatomical labeling of activations in SPM using a macroscopic anatomical parcellation of the MNI MRI single-subject brain. *NeuroImage*. 2002;15(1):273–89.
39. Seeley WW, Crawford RK, Zhou J, Miller BL, Greicius MD. Neurodegenerative diseases target large-scale human brain networks. *Neuron*. 2009;62(1):42–52.
40. Zhang Y, Tartaglia MC, Schuff N, Chiang GC, Ching C, Rosen HJ, et al. MRI signatures of brain macrostructural atrophy and microstructural degradation in frontotemporal lobar degeneration subtypes. *J Alzheimer's Dis*. 2013;33(2):431–44.
41. Ossenkoppele R, Schonhaut DR, Scholl M, Lockhart SN, Ayakta N, Baker SL, et al. Tau PET patterns mirror clinical and neuroanatomical variability in Alzheimer's disease. *Brain*. 2016;139(Pt 5):1551–67.
42. Wang Y, Shi Z, Zhang N, Cai L, Li Y, Yang H, et al. Spatial patterns of hypometabolism and amyloid deposition in variants of Alzheimer's disease corresponding to brain networks: a prospective cohort study. *Mol Imaging Biol*. 2019;21(1):140–8.
43. La Joie R, Perrotin A, Barre L, Hommet C, Mezenge F, Ibazizene M, et al. Region-specific hierarchy between atrophy, hypometabolism, and beta-amyloid (Abeta) load in Alzheimer's disease dementia. *J Neurosci*. 2012;32(46):16265–73.
44. Woodward MC, Rowe CC, Jones G, Villemagne VL, Varos TA. Differentiating the frontal presentation of Alzheimer's disease with FDG-PET. *J Alzheimer's Dis*. 2015;44(1):233–42.
45. Saxe R, Moran JM, Scholz J, Gabrieli J. Overlapping and non-overlapping brain regions for theory of mind and self reflection in individual subjects. *Soc Cogn Affect Neurosci*. 2006;1(3):229–34.
46. Schacter DL, Addis DR, Buckner RL. Remembering the past to imagine the future: the prospective brain. *Nat Rev Neurosci*. 2007;8(9):657–61.
47. Frodl T, Meisenzahl EM, Zetzsche T, Born C, Jager M, Groll C, et al. Larger amygdala volumes in first depressive episode as compared to recurrent major depression and healthy control subjects. *Biol Psychiatry*. 2003;53(4):338–44.
48. Groen W, Teluij M, Buitelaar J, Tendolcar I. Amygdala and hippocampus enlargement during adolescence in autism. *J Am Acad Child Adolesc Psychiatry*. 2010;49(6):552–60.
49. Townley RA, Graff-Radford J, Mantyh WG, Botha H, Polsinelli AJ, Przybelski SA, et al. Progressive dysexecutive syndrome due to Alzheimer's disease: a description of 55 cases and comparison to other phenotypes. *Brain Commun*. 2020;2(1):fcaa068.
50. Seeley WW, Carlin DA, Allman JM, Macedo MN, Bush C, Miller BL, et al. Early frontotemporal dementia targets neurons unique to apes and humans. *Ann Neurol*. 2006;60(6):660–7.

## Publisher's Note

Springer Nature remains neutral with regard to jurisdictional claims in published maps and institutional affiliations.